

## Effect of Zr Content on the Activity of 5%CuO/Ce<sub>1-x</sub>Zr<sub>x</sub>O<sub>2</sub> Catalysts in CO Oxidation by Oxygen in the Excess of Hydrogen

A. N. Il'ichev<sup>a, \*</sup>, M. Ya. Bykhovsky<sup>a</sup>, Z. T. Fattakhova<sup>a</sup>, D. P. Shashkin<sup>a</sup>, Yu. E. Fedorova<sup>b</sup>,  
V. A. Matyshak<sup>a</sup>, and V. N. Korchak<sup>a</sup>

<sup>a</sup>*Semenov Institute of Chemical Physics, Russian Academy of Sciences, Moscow, 119991 Russia*

<sup>b</sup>*Boreshkov Institute of Catalysis, Siberian Branch, Novosibirsk, 630090 Russia*

\**e-mail: Ilichev-alix@yandex.ru*

Received December 25, 2018; revised February 20, 2019; accepted April 17, 2019

**Abstract**—The article reports the synthesis of 5%CuO/Ce<sub>1-x</sub>Zr<sub>x</sub>O<sub>2</sub> catalysts based on CeO<sub>2</sub>, ZrO<sub>2</sub> oxides and Ce<sub>1-x</sub>Zr<sub>x</sub>O<sub>2</sub> solid solutions with  $x = 0.2, 0.5,$  and  $0.8$ . It is found that copper oxide is present in the catalysts in a highly dispersed form. In strong interaction with supports, it forms active oxygen, which participates in CO chemisorption and low-temperature oxidation of CO in the presence of hydrogen. In selective CO oxidation, the highest conversion ( $\gamma_{\max} = 100\%$ ) was obtained at temperatures of 120–160°C in the presence of 5%CuO/CeO<sub>2</sub>. In the modification of CeO<sub>2</sub> by zirconium cations, the conversion on 5%Ce<sub>0.5</sub>Zr<sub>0.5</sub>O<sub>2</sub> decreases to 92% at 160°C because oxygen binding strengthens on copper-containing sites. On the 5%CuO/ZrO<sub>2</sub> sample, the maximum conversion is 67% at 180°C. The modification of ZrO<sub>2</sub> by cerium cations leads to an increase in the conversion to 87% at 160°C on the 5%CuO/Ce<sub>0.2</sub>Zr<sub>0.8</sub>O<sub>2</sub> sample as a result of increasing the amount of oxygen vacancies in the support. Taking into account the properties of CO complexes formed on copper-containing oxidation and adsorption sites, and the interaction of these complexes with adsorbed oxygen, their participation in the reaction of low-temperature CO oxidation by oxygen in excess of hydrogen on 5%CuO/CeO<sub>2</sub> and 5%CuO/ZrO<sub>2</sub> catalysts is considered.

**Keywords:** oxides, solid solutions, CO oxidation

**DOI:** 10.1134/S002315841905001X

### INTRODUCTION

The CuO/CeO<sub>2</sub> catalysts have a high activity in the reaction of selective oxidation of CO with oxygen in excess of hydrogen at low temperatures. After modifying and adapting to industrial conditions of H<sub>2</sub> purification from CO, they can replace expensive systems containing Pt, Pd, Ir, Rh, and Ru, which will reduce the cost of this process [1]. High purity of hydrogen with a CO concentration lower than 10 ppm is necessary for the generation of power energy by the oxidation of H<sub>2</sub> by oxygen in air in platinum-containing fuel cells. In the future, such an efficient and environmentally friendly way to generate power energy can be used in car manufacturing and heat power industry for domestic household [2, 3].

The activity of the CuO/CeO<sub>2</sub> catalyst in the oxidation of CO by oxygen in a hydrogen-containing mixture is explained by a synergistic effect of interaction between CuO and CeO<sub>2</sub> oxides, which are more easily reduced and oxidized than each of them separately [3, 4]. To increase the catalyst selectivity in CO oxidation in the presence of hydrogen, an important task is to shift the temperature range of the maximum CO conversion toward low temperatures. It can be

solved by modifying copper sites with metal ions with suitable redox properties [5] or by improving the properties of the support by adding other oxides to CeO<sub>2</sub> [6].

Thus, it is known from [7] that the introduction of zirconium into the structure of cerium oxide, Ce<sub>1-x</sub>Zr<sub>x</sub>O<sub>2</sub> solid solutions with a stable structure and a certain crystallite size are formed. Compared with CeO<sub>2</sub>, they have redox properties combined with high thermal stability, the ability to accumulate and evolve oxygen, and also provide a high dispersity of the deposited metal on the surface. The literature data on the efficiency of copper-containing CuO/Ce<sub>1-x</sub>Zr<sub>x</sub>O<sub>2</sub> catalysts for the reaction of selective oxidation of CO are controversial and differ depending on the content of zirconium ions in the samples and methods of support preparation [8–11]. Of greatest interest are the works [8, 10], which reported the activity of CuO/Ce<sub>0.8</sub>Zr<sub>0.2</sub>O<sub>2</sub> and CuO(5%)–CeO(47.5%)–ZrO<sub>2</sub>(47.5%) catalysts comparable with and even higher than that of CuO/CeO<sub>2</sub>.

In [12–14], we studied the low-temperature oxidation of CO by oxygen in a hydrogen-containing mixture on CuO/CeO<sub>2</sub> and CuO/ZrO<sub>2</sub> catalysts with different contents of deposited copper oxide and showed that the conversion of CO to CO<sub>2</sub> reaches 98.5% at

150°C on the sample (5–6.4)% CuO/CeO<sub>2</sub> and is lower than 87% at 160°C in the presence of 5%CuO/ZrO<sub>2</sub>. We also found that the activity of CuO/ZrO<sub>2</sub> depends on the phase composition of the support. Thus, copper oxide on the tetragonal-phase ZrO<sub>2</sub>(t) is much more active than on the monoclinic-phase ZrO<sub>2</sub>(m) both in adsorption and in the selective oxidation of CO. Although the amount of chemisorbed CO at 20°C on the 5%CuO/ZrO<sub>2</sub>(t) sample was the same as that on 5%CuO/CeO<sub>2</sub>, its activity in CO oxidation in the presence of hydrogen was lower. Samples 5%CuO/CeO<sub>2</sub>, 5%CuO/ZrO<sub>2</sub>, and 5%CuO/Zr<sub>0.5</sub>Ce<sub>0.5</sub> prepared by the microemulsion method with a crystallite size  $d = 5$  nm, were less active than the crystallites of the same composition with  $d = 15$ – $20$  nm prepared by the pyrolysis of nitric acid salts.

In this work, we carried out a detailed study of the effect of Ce and Zr ions in the structure of the CeO<sub>2</sub> and ZrO<sub>2</sub> supports of copper-containing catalysts on the activity and selectivity in the oxidation of CO by oxygen in the presence of hydrogen has been carried out.

## EXPERIMENTAL

Ce<sub>1-x</sub>Zr<sub>x</sub>O<sub>2</sub> supports with  $x = 0, 0.2, 0.5, 0.8,$  and  $1$  were synthesized by the Pechini method according to [15]. The resulting powders were impregnated at 20°C by a solution of copper nitrate Cu(NO<sub>3</sub>)<sub>2</sub> · 3H<sub>2</sub>O in such a concentration that the CuO content of the final product was 5 wt %. Upon impregnation the samples were dried in air by increasing the temperature to 500°C with a rate of 10°C/min, and then kept 500°C for 1 h.

The specific surface area of the samples ( $S_{sp}$ ) was determined by the BET method of low-temperature argon adsorption. XRD patterns were recorded on a DRON-3M instrument (Burevestnik, Russia) in the range of  $2\theta$  angle from 8° to 90°. The phase composition and lattice parameters were found by comparing the obtained diffraction patterns with JCPDS data [16]. The average crystallite size was estimated using the Debye–Scherer formula for the line with the maximum intensity. The average value of the unit cell parameter was determined from the lines of XRD pattern of the sample [17].

The oxidation of CO by oxygen in the excess of hydrogen was carried out on a flow-type setup. A sample (a mixture containing 50 mg of catalyst powder and 70 mg of a quartz powder with a fraction of 0.10–0.25 mm) was placed in a quartz reactor (a tube with an inner diameter of 3 mm) and calcined in a flow of oxygen at 500°C for 20 min. Then, the reactor was cooled to 40°C and the oxygen flow was replaced with the reaction mixture 98 vol % H<sub>2</sub> + 1 vol % CO + 1 vol % O<sub>2</sub>. The mixture was fed into the reactor at a rate of 20 mL/min. The catalyst activity was evaluated by the conversion of CO to CO<sub>2</sub> at different temperatures.

The temperature was increased in a stepwise manner with temperature increments of 20°C. The reaction products were separated on columns with 13X molecular sieves and silica gel and detected using a thermal conductivity detector on a Kristall 2000M chromatograph (Khromatek, Russia).

The interaction of samples with hydrogen were studied by TPR-H<sub>2</sub> in a flow of the 6% H<sub>2</sub> mixture with Ar (30 mL/min) when heating the sample at a rate of 5°C/min from 30 to 700°C. The sample (100 mg) was placed in a U-shaped reactor, calcined in a flow of oxygen at 500°C for 10 min, cooled to 30°C, and then replaced the flow of oxygen by a hydrogen mixture and recorded a TPR-H<sub>2</sub> profile using the thermal conductivity detector. The amount of consumed hydrogen was determined from the TPR-H<sub>2</sub> peak area comparing it with the corresponding value obtained for the reference (NiO).

Carbon oxide adsorption and oxidation was studied by TPD CO in a vacuum. The sample (100 mg) was preliminarily vacuumed at 20°C, heated at 500°C and a residual pressure of 10<sup>-4</sup> Pa for 1 h, and then oxygen was fed into the reactor to a pressure of  $P = 3 \times 10^2$  Pa. The reactor was allowed to stay for 20 min, and then it was cooled to room temperature and vacuumed. Hereafter, the resulting catalyst is called **oxidized**. After that, CO was adsorbed on it at  $P = 3.3 \times 10^3$  Pa and 20°C for 10 min, the gas was evacuated for 20 min, and TPD CO profiles were recorded under constant vacuum conditions at a sample heating rate of 10°C/min. The change in pressure in the TPD CO profile reflects the temperature dependence of the desorption rate  $w$ . The pressure was recorded with an automated Pirani pressure gauge [18]. In order to isolate the peaks of CO desorption and oxidation product (CO<sub>2</sub>) desorption in the TPD spectrum, carbon dioxide was frozen in a U-shaped trap placed between the sample and the gauge and cooled with liquid nitrogen. Such a technique made it possible to record the profiles of the joint CO + CO<sub>2</sub> desorption and separate CO desorption. The subtraction of the second profile from the first one made it possible to obtain the profile of CO<sub>2</sub> desorption. The amount of desorbed CO<sub>2</sub> ( $N_{des.CO_2}$ ) was determined from the CO<sub>2</sub> pressure of after it was thawed out, and the amount of desorbed CO ( $N_{des.CO}$ ) was calculated using the balance equation:  $N_{des.CO} = N_{ads.CO} - N_{des.CO_2} = N_{des.CO+CO_2} - N_{des.CO_2}$ . When performing the calculations, we proceeded either from a known amount of adsorbed CO ( $N_{ads.CO}$ ), or from the total amount of desorbed gas  $N_{des.CO+CO_2}$  found in a separate TPD experiment in a closed reactor without evacuation. The accuracy of  $N_{des.CO+CO_2}$  and  $N_{ads.CO}$  determination corresponded to the accuracy of gas pressure measurement and was 20%.

Gaseous CO and O<sub>2</sub> prepared according to the procedures described in [19] were used in adsorption

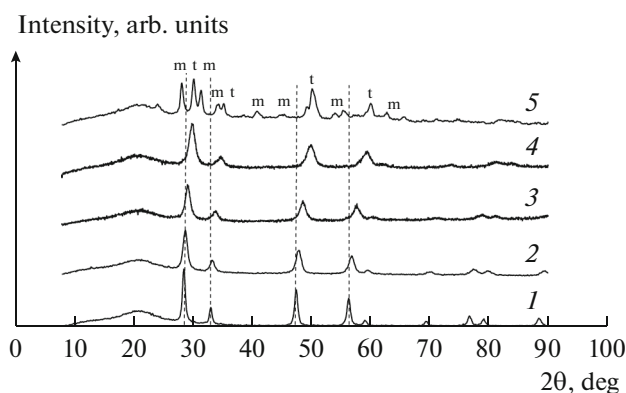


**Fig. 1.** XRD patterns of  $\text{CeO}_2$  (1),  $\text{Ce}_{0.8}\text{Zr}_{0.2}\text{O}_2$  (2),  $\text{Ce}_{0.5}\text{Zr}_{0.5}\text{O}_2$  (3),  $\text{Ce}_{0.2}\text{Zr}_{0.8}\text{O}_2$  (4) and  $\text{ZrO}_2(\text{m} + \text{t})$  (5) samples.

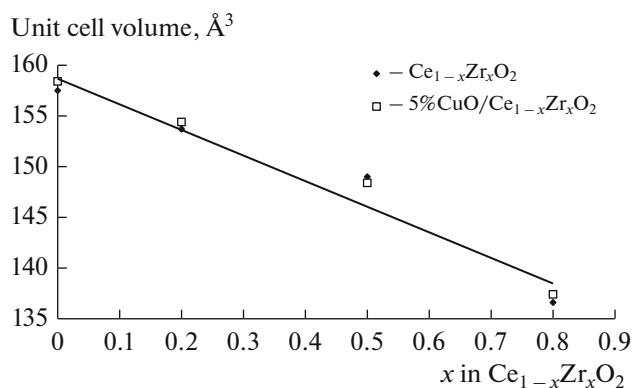


**Fig. 2.** Dependence of the unit cell volume on the  $\text{Zr}^{4+}$  content of  $\text{Ce}_{1-x}\text{Zr}_x\text{O}_2$  and 5%CuO/ $\text{Ce}_{1-x}\text{Zr}_x\text{O}_2$  solid solutions.

studies. To eliminate uncontrolled impurities, they were introduced onto the sample through a trap cooled with liquid nitrogen.

## RESULTS

### Sample Characterization

Figure 1 shows XRD patterns of synthesized  $\text{Ce}_{1-x}\text{Zr}_x\text{O}_2$  samples. It can be seen from XRD patterns 1–4 that the samples have a cubic (c) modification [20]. As the zirconium content of samples increases, the reflections shift to large values of the  $2\theta$  angles due to a decrease in the lattice parameter  $a$  ( $\text{Å}$ ) of the cubic unit cell. In samples with  $x = 0, 0.2, 0.5,$  and  $0.8$ , the lattice parameters are 5.41, 5.37, 5.30, and 5.15  $\text{Å}$ , respectively. Figure 2 shows the dependence of the cell volume  $a^3$  on  $x$ , which has a linear form. According to [20–22], the values of cell parameters and the linear dependence of its volume on  $x$  confirm the formation of solid solutions with a cubic modification. XRD pattern 5 corresponds to zirconium oxide consisting of a mixture of monoclinic and tetragonal phases (m + t).

It follows from Table 1 that  $\text{Ce}_{1-x}\text{Zr}_x\text{O}_2$  samples have  $S_{\text{sp}} \approx 30\text{--}60 \text{ m}^2/\text{g}$  and a crystallite size of 7–13 nm. The deposition of copper oxide leads to a decrease in the specific surface area of solid solutions by 25–50% but does not affect the size of crystallites. The XRD patterns of 5%CuO/ $\text{Ce}_{1-x}\text{Zr}_x\text{O}_2$  samples coincide with those of  $\text{Ce}_{1-x}\text{Zr}_x\text{O}_2$  supports. The absence of CuO reflections on them indicates its high dispersion. The interaction of copper oxide with the support does not change the unit cell parameters of the supports (Fig. 2); therefore, the deposition of copper oxide on the  $\text{Ce}_{1-x}\text{Zr}_x\text{O}_2$  supports probably reduces their porosity.

The effect of zirconium content on the properties of oxygen in  $\text{Ce}_{1-x}\text{Zr}_x\text{O}_2$  and in copper-containing

sites of 5%CuO/ $\text{Ce}_{1-x}\text{Zr}_x\text{O}_2$  catalysts was studied using the TPR- $\text{H}_2$  method.

### Temperature-Programmed Reduction of $\text{Ce}_{1-x}\text{Zr}_x\text{O}_2$ and 5%CuO/ $\text{Ce}_{1-x}\text{Zr}_x\text{O}_2$ Samples by Hydrogen

Figure 3 shows the TPR- $\text{H}_2$  profiles of preliminarily oxidized  $\text{Ce}_{1-x}\text{Zr}_x\text{O}_2$  samples. Profile 1 of cerium oxide is complex and has peaks of hydrogen absorption with maxima at 360 and 510°C. According to [22], they are due to the reduction of nonstoichiometric oxide  $\text{CeO}_x$ . The total amount of absorbed hydrogen per square meter of oxide ( $N_{\text{H}_2}$ ) was determined as the amount of absorbed hydrogen for 1 g of the catalyst divided by the value of its specific surface area. As can be seen from Table 1, for  $\text{CeO}_2$ , it is  $0.08 \times 10^{-4} \text{ mol}/\text{m}^2$  and is close to the stoichiometric amount of oxygen ions on the surface,  $0.1 \times 10^{-4} \text{ mol}/\text{m}^2$ . This fact suggests that, hydrogen is oxidized by surface oxygen in the temperature range 300–600°C since the oxidation of hydrogen by oxygen from the bulk of  $\text{CeO}_2$  oxide occurs at  $T > 700^\circ\text{C}$ . In profiles 2 and 3 of samples  $\text{Ce}_{0.8}\text{Zr}_{0.2}\text{O}_2$  and  $\text{Ce}_{0.5}\text{Zr}_{0.5}\text{O}_2$ , the peak maxima are observed at higher temperatures (550 and 570°C), and the amount of hydrogen absorbed by the samples increases to  $0.26 \times 10^{-4}$  and  $0.18 \times 10^{-4} \text{ mol}/\text{m}^2$ , respectively. In this case, surface and near-surface oxygen of solid solutions participate in the reaction [23, 24]. Profile 4 of sample  $\text{Ce}_{0.2}\text{Zr}_{0.8}\text{O}_2$  contains peaks at 375 and 540°C. The total amount of hydrogen absorbed by this sample is close to the amount of oxygen ions on the surface, and the area of the first peak (and, therefore, the amount of hydrogen) is larger than the second one. The high-temperature peak at 540°C can be associated with the absorption of hydrogen in the surface layer. The nature of the peak at 375°C is unclear. A similar peak was observed in [14] in the TPR- $\text{H}_2$  profile of the  $\text{Ce}_{0.5}\text{Zr}_{0.5}\text{O}_2$  sample with

**Table 1.** Characteristics of samples

Sample	$S_{\text{sp}}$ , m <sup>2</sup> /g	Crystallite size, nm	$N_{\text{H}_2} \times 10^4$ mol/m <sup>2</sup>	$N_{\text{p}} \times 10^4$ , mol/m <sup>2</sup>	$N_{\text{H}_2}/N_{\text{p}}$
CeO <sub>2</sub>	37	8.0	0.08	—	—
Ce <sub>0.8</sub> Zr <sub>0.2</sub> O <sub>2</sub>	32	7.4	0.26	—	—
Ce <sub>0.5</sub> Zr <sub>0.5</sub> O <sub>2</sub>	54	10.3	0.18	—	—
Ce <sub>0.2</sub> Zr <sub>0.8</sub> O <sub>2</sub>	56	8.7	0.12	—	—
ZrO <sub>2</sub>	20	13.0	0	—	—
CuO/CeO <sub>2</sub>	35	7.5	0.31	0.18	1.7
CuO/Ce <sub>0.8</sub> Zr <sub>0.2</sub> O <sub>2</sub>	29	11.0	0.5	0.21	2.4
CuO/Ce <sub>0.5</sub> Zr <sub>0.5</sub> O <sub>2</sub>	27	9.6	0.47	0.23	2
CuO/Ce <sub>0.2</sub> Zr <sub>0.8</sub> O <sub>2</sub>	42	8.4	0.20	0.15	1.3
CuO/ZrO <sub>2</sub>	20	13.0	0.37	0.31	1.2

Dashes mean the absence of copper oxide.

a crystallite size of ~5 nm. The authors explained its presence by lowering the energy of oxygen binding to the surface due to a decrease in the size of crystallites. The absence of hydrogen absorption peaks in profile 5 for ZrO<sub>2</sub> indicates the high strength of the oxygen bond in it. The absorption of hydrogen by zirconium oxide at 730°C was noted in [25].

TPR-H<sub>2</sub> curves of the 5%CuO/Ce<sub>1-x</sub>Zr<sub>x</sub>O<sub>2</sub> samples in Fig. 4 do not contain peaks present in the support profiles. This suggests that the peaks on these profiles are associated with the reduction of copper oxide. The overall amounts of 5%CuO/Ce<sub>1-x</sub>Zr<sub>x</sub>O<sub>2</sub> absorbed in TPR experiments for hydrogen are compared in Table 1 with the amount of hydrogen  $N_{\text{r}}$  calculated according to the reaction  $\text{CuO} + \text{H}_2 = \text{Cu}^0 + \text{H}_2\text{O}$  under the assumption that all copper cations in the oxidized samples are in the Cu<sup>2+</sup> state [26, 27]. It is seen from the  $N_{\text{H}_2}/N_{\text{p}}$  ratio that the amounts of samples with  $x = 0-0.5$  are greater than the amount of hydrogen needed to reduce copper oxide in them.

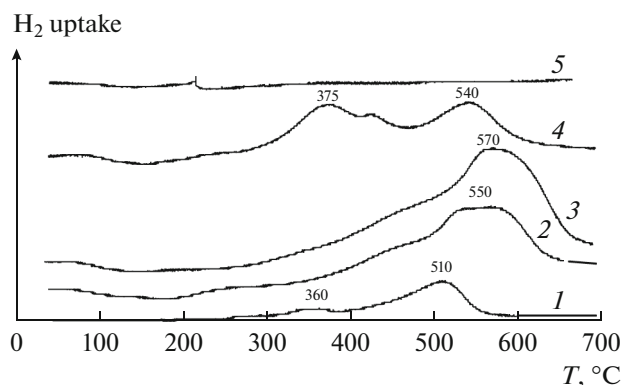


**Fig. 3.** TPR-H<sub>2</sub> profiles for CeO<sub>2</sub> (1), Ce<sub>0.8</sub>Zr<sub>0.2</sub>O<sub>2</sub> (2), Ce<sub>0.5</sub>Zr<sub>0.5</sub>O<sub>2</sub> (3), Ce<sub>0.2</sub>Zr<sub>0.8</sub>O<sub>2</sub> (4), ZrO<sub>2</sub> (5) samples.

Excessive absorption of H<sub>2</sub> indicates the reduction of copper oxide together with supports. For 5%CuO/ZrO<sub>2</sub> and 5%CuO/Ce<sub>0.2</sub>Zr<sub>0.8</sub>O<sub>2</sub> samples, similar values of  $N_{\text{H}_2}$  and  $N_{\text{r}}$  were obtained, which indicate the preferential reduction of copper oxide in them.

In profile 1 of the 5%CuO/CeO<sub>2</sub> sample, there are two peaks with maxima at 145 and 180°C, which are lower than the reduction temperature of the CuO(m) phase (320°C, profile 6). They are attributed to the reduction of two forms of highly dispersed CuO oxide according to [28–32]. According to [9], only CuO can be reduced at 145°C, and CuO together with CeO<sub>2</sub> can be reduced at 180°C. A decrease in the reduction temperature of the interacting CuO and CeO<sub>2</sub> oxides in comparison with those for these oxides separately (maximum at  $T > 300^\circ\text{C}$ ) is due to the synergistic effect. The low-temperature reduction by hydrogen atoms of the support, which is inactive in H<sub>2</sub> adsorption at 180°C, occurs more easily with their spillover from copper, which is formed at 145°C [28].

In the profiles 2 and 3 of the 5%CuO/Ce<sub>1-x</sub>Zr<sub>x</sub>O<sub>2</sub> samples with  $x = 0.2$  and  $0.5$ , peaks of hydrogen absorption are separated and shift toward higher temperatures relative to the peaks in profile 1. Thus, in the 5%CuO/Ce<sub>0.8</sub>Zr<sub>0.2</sub>O<sub>2</sub> sample, two forms of copper oxide are reduced by hydrogen with maxima on the TPR-H<sub>2</sub> curves at 163 and 268°C (profile 2). The authors of [9, 33] believe that the first form is the result of the strong interaction of highly dispersed CuO and support, and the second form corresponds to particles of the CuO phase that are weakly bound to the surface. In the 5%CuO/Ce<sub>0.5</sub>Zr<sub>0.5</sub>O<sub>2</sub> sample, these two forms of copper oxide are reduced at 194 and 370°C (profile 3). An increase in the reduction temperature can be associated with increasing copper oxide particle size with a decrease in the surface area of the samples upon supporting CuO (Table 1). To check this assumption we

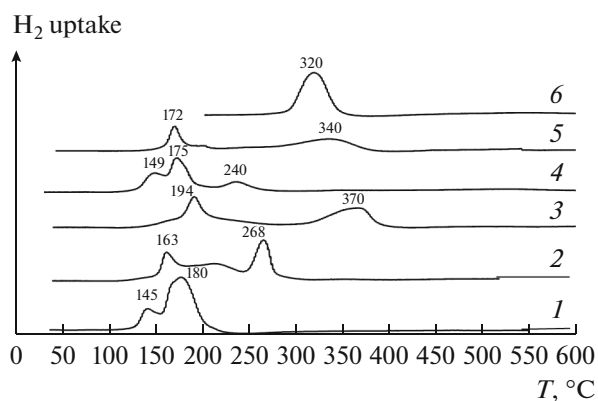


**Fig. 4.** TPR- $H_2$  profiles for 5%CuO/CeO<sub>2</sub> (1), 5%CuO/Ce<sub>0.8</sub>Zr<sub>0.2</sub>O<sub>2</sub> (2), 5%CuO/Ce<sub>0.5</sub>Zr<sub>0.5</sub>O<sub>2</sub> (3), 5%CuO/Ce<sub>0.2</sub>Zr<sub>0.8</sub>O<sub>2</sub> (4), 5%CuO/ZrO<sub>2</sub> (5), CuO (6) samples.

studied the 5%CuO/Ce<sub>0.5</sub>Zr<sub>0.5</sub>O<sub>2</sub> sample with  $S_{sp} = 65 \text{ m}^2/\text{g}$  in which support—a solid solution of Ce<sub>0.5</sub>Zr<sub>0.5</sub>O<sub>2</sub>—was prepared by coprecipitation of salts according to the method [33]. The TPD- $H_2$  profile for this sample was not different from profile 3. On the other hand, profiles 2 and 3 for 5%CuO/Ce<sub>0.8</sub>Zr<sub>0.2</sub>O<sub>2</sub> and 5%CuO/Ce<sub>0.5</sub>Zr<sub>0.5</sub>O<sub>2</sub> samples with close  $S_{sp}$  (29 and 27  $\text{m}^2/\text{g}$ , respectively) are different. Therefore, specific features of CuO reduction in the 5%CuO/Ce<sub>0.5</sub>Zr<sub>0.5</sub>O<sub>2</sub> and 5%CuO/Ce<sub>0.8</sub>Zr<sub>0.2</sub>O<sub>2</sub> catalysts are not related to the values of their specific surface area and depend on their structural properties, which change depending on the composition of cations in the solid solution. This makes it possible to assume that an increase in the reduction temperature from 163 to 194°C with an increase in the zirconium content of the 5%CuO/Ce<sub>0.8</sub>Zr<sub>0.2</sub>O<sub>2</sub> sample is due to the strengthening of its interaction with supports. The reduction of the 5%CuO/Ce<sub>0.5</sub>Zr<sub>0.5</sub>O<sub>2</sub> sample at ~370°C can be due to particles of the Cu<sub>2</sub>O phase [30] and support (see Fig. 3).

For the 5%CuO/Ce<sub>0.2</sub>Zr<sub>0.8</sub>O<sub>2</sub>(c) catalyst in which  $N_{Zr} > N_{Ce}$ , the temperature of copper oxide reduction decreases (profile 4). There are three peaks on the TPD- $H_2$  curve for this sample. Peaks with maxima at 149 and 175°C correspond to the reduction of CuO clusters and a peak at 240°C, to the particles of the CuO phase [13, 34]. In profile 5 of the 5%CuO/ZrO<sub>2</sub>(m + t) sample at 172°C, clusters of copper oxide on the ZrO<sub>2</sub>(t) crystallites are reduced, and a peak at 340°C refers to copper oxide reduction in ZrO<sub>2</sub>(m) [13].

The presented data show that hydrogen is more easily oxidized by oxygen in the near-surface layer of the Ce<sub>1-x</sub>Zr<sub>x</sub>O<sub>2</sub> solid solutions than by oxygen from the bulk of CeO<sub>2</sub> oxide. For the 5%CuO/Ce<sub>1-x</sub>Zr<sub>x</sub>O<sub>2</sub> ( $x = 0-0.5$ ) samples, a synergistic effect is observed, which weakens with increasing  $x$ : the temperature of

the joint reduction of copper oxide and supports increases with increasing Zr cation content of the support. At  $x > 0.5$ , the synergistic effect is negligible. In these cases, the reduction temperature of copper oxide depends on the specific features of its interaction with the surface of crystallites of different phase composition in the Ce<sub>0.2</sub>Zr<sub>0.8</sub>O<sub>2</sub>(c) and ZrO<sub>2</sub>(m + t) samples.

#### CO Oxidation by Oxygen in the Excess of $H_2$ on 5%CuO/Ce<sub>1-x</sub>Zr<sub>x</sub>O<sub>2</sub>

Figure 5 shows the dependences of CO conversion to CO<sub>2</sub> ( $\gamma$ ) on temperature  $T$  for the 5%CuO/Ce<sub>1-x</sub>Zr<sub>x</sub>O<sub>2</sub> catalysts in hydrogen containing mixture CO + O<sub>2</sub> + H<sub>2</sub>. It is seen that for 5%CuO/CeO<sub>2</sub>, the conversion of CO increases from 0 to a maximum value of  $\gamma_{max} = 98-100\%$  with changing temperature from 40 to 120°C (curve 1). A conversion of 100% is preserved at 120–160°C and then decreases to 70% at 220°C. Similar  $\gamma(T)$  dependences are observed for other samples (curves 2–5). It follows from data presented in Fig. 5 that, with an increase in the fraction of Zr in the catalysts from 0.2 to 1, the reaction temperature increases with a simultaneous decrease in the conversion. The  $\gamma_{max}(T)$  dependence on the Zr content of the catalyst makes it possible to construct the following activity series: 5%CuO/CeO<sub>2</sub> (100%, 120–160°C) > 5%CuO/Ce<sub>0.8</sub>Zr<sub>0.2</sub>O<sub>2</sub> (98%, 160°C) > 5%Ce<sub>0.5</sub>Zr<sub>0.5</sub>O<sub>2</sub> (92%, 160°C) > 5%CuO/Ce<sub>0.2</sub>Zr<sub>0.8</sub>O<sub>2</sub> (87%, 160°C) > 5%CuO/ZrO<sub>2</sub> (67%, 180°C).

Simultaneously with the CO conversion, the conversion of O<sub>2</sub> was measured. The dependences of the conversion of CO and O<sub>2</sub> on temperature for the 5%CuO/CeO<sub>2</sub> and 5%CuO/ZrO<sub>2</sub> samples are compared in Fig. 6. Thus, on the 5%CuO/CeO<sub>2</sub> sample, the oxidation of CO begins at 60°C. When the temperature rises to 120°C, the reaction occurs with 100% selectivity, since under these conditions the ratio of the amounts of CO and O<sub>2</sub> molecules consumed corresponds to their ratio obtained from the reaction equation  $\text{CO} + 0.5\text{O}_2 \rightarrow \text{CO}_2$  (compare Fig. 6, curves 1 and 1'). At 100–120°C, oxygen absorption slows down with a decrease in the CO content of the stream. At 120°C, the O<sub>2</sub> conversion is 50% at a CO conversion close to 100%. When the temperature rises to 160°C, the O<sub>2</sub> conversion increases due to the participation of oxygen in hydrogen oxidation, and the CO conversion remains unchanged and is 100%. At  $T \geq 160^\circ\text{C}$ , oxygen from the mixture is completely consumed by two reactions. Under these conditions of the competition for oxygen, the conversion of CO decreases to 70% (220°C) due to the increasing rate of oxygen consumption in the reaction with hydrogen relative to the rate of its consumption in the reaction with carbon dioxide.

In the case of the 5%CuO/ZrO<sub>2</sub> sample, the reactions of CO and H<sub>2</sub> oxidation begin almost simultane-

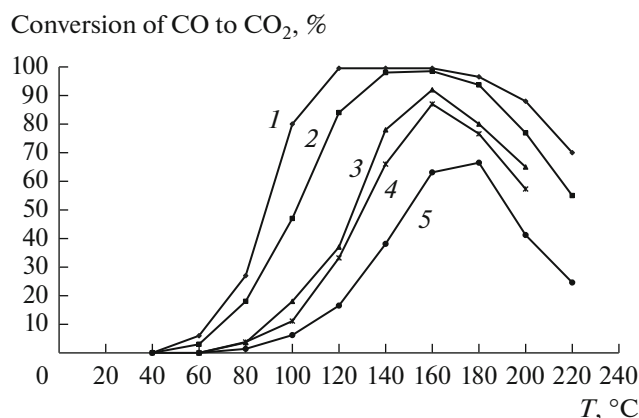


**Fig. 5.** Temperature dependence of the CO conversion into  $\text{CO}_2$  on temperature for 5%CuO/ $\text{CeO}_2$  (1), 5%CuO/ $\text{Ce}_{0.8}\text{Zr}_{0.2}\text{O}_2$  (2), 5%CuO/ $\text{Ce}_{0.5}\text{Zr}_{0.5}\text{O}_2$  (3), 5%CuO/ $\text{Ce}_{0.2}\text{Zr}_{0.8}\text{O}_2$  (4), 5%CuO/ $\text{ZrO}_2$  (5) samples.

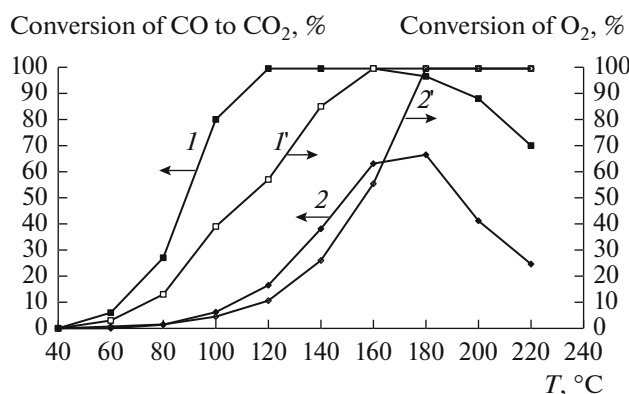


**Fig. 6.** Temperature dependence of the CO (1, 2) and  $\text{O}_2$  (1', 2') conversion for 5%CuO/ $\text{CeO}_2$  (1, 1') and 5%CuO/ $\text{ZrO}_2$  (2, 2') samples.

ously, since at the initial stage of the process (100–140°C) oxygen consumption is higher than that spent on CO oxidation (compare Fig. 6, curves 2 and 2'). Due to the higher rate of oxygen consumption in the oxidation of hydrogen than in the oxidation of CO at 160–220°C, the conversion of CO to  $\text{CO}_2$  reaches only 67% at 180°C and then decreases to 20% at 220°C. That is, in the entire temperature range 100–220°C, the selectivity to the formation of  $\text{CO}_2$  is below 100%.

Thus, an increase in the content of Zr cations in  $\text{CeO}_2$  lowers the activity of 5%CuO/ $\text{Ce}_{1-x}\text{Zr}_x\text{O}_2$  catalysts in CO oxidation by oxygen in the excess of hydrogen: the temperature of the onset of the reaction increases, the conversion of  $\gamma_{\text{max}}$  decreases with a shift of the corresponding temperature toward higher temperatures. The drop of activity is due to the competition for oxygen in CO and  $\text{H}_2$  oxidation reactions. The lowest activity was observed for the 5%CuO/ $\text{ZrO}_2$ (m + t) cata-

lyst. When modifying the  $\text{ZrO}_2$  structure by a small amount of cerium, the activity of 5%CuO/ $\text{Ce}_{0.2}\text{Zr}_{0.8}\text{O}_2$  catalyst increases from 67% (180°C) to 87% (160°C).

The activated nature of the reaction of selective oxidation of CO may be due to the transformation of surface intermediates formed during the adsorption of CO and  $\text{O}_2$ . To determine their nature, the forms of CO adsorption, their thermal stability, and the effect of oxygen adsorption on them were studied.

#### CO Oxidation by Oxygen from the Catalyst and Oxygen Adsorbed on 5%CuO/ $\text{Ce}_{1-x}\text{Zr}_x\text{O}_2$

Figure 7 shows the TPD CO curves for the oxidized 5%CuO/ $\text{Ce}_{1-x}\text{Zr}_x\text{O}_2$  samples after CO is adsorbed on them at  $P = 3.3 \times 10^3$  Pa for 10 min and evacuated for 20 min at 20°C. Profiles 1–5 are formed during desorption of CO and  $\text{CO}_2$  from the sites of adsorption and oxidation, respectively.

Data on the amount of CO and  $\text{CO}_2$  molecules desorbed per square meter of the sample, and temperatures  $T_{\text{max}}$  corresponding to the maximum rates of gas desorption are presented in Table 2. Based on the results obtained earlier in [26, 27], it can be assumed that profiles 1 and 5 for 5%CuO/ $\text{CeO}_2$  and 5%CuO/ $\text{ZrO}_2$  samples are formed by the decomposition of one and two types of linear carbonyl complexes  $\text{Cu}^+ - \text{CO}$  with CO desorption and bridge mono- and bidentate carbonate complexes with  $\text{CO}_2$  desorption in different specific temperature regions. Profiles 2–4 of the 5%CuO/ $\text{Ce}_{1-x}\text{Zr}_x\text{O}_2$  samples with  $x = 0.2, 0.5$ , and 0.8 are similar to TPD CO profiles 1 and 5. Therefore, these catalysts form the same carbonyl and carbonate structures as 5%CuO/ $\text{CeO}_2$  and 5%CuO/ $\text{ZrO}_2$ . The close temperature regions of CO and  $\text{CO}_2$  desorption and the values of  $T_{\text{max}}$  in profiles 4 and 5 indicate that carbonyl and carbonate structures are identical in 5%CuO/ $\text{ZrO}_2$  and 5%CuO/ $\text{Ce}_{0.2}\text{Zr}_{0.8}\text{O}_2$ . Identical carbonyls of two types are also found in 5%CuO/ $\text{Ce}_{0.8}\text{Zr}_{0.2}\text{O}_2$ , 5%CuO/ $\text{Ce}_{0.5}\text{Zr}_{0.5}\text{O}_2$ , and 5%CuO/ $\text{Ce}_{0.2}\text{Zr}_{0.8}\text{O}_2$  samples (profiles 1–3). This is not the case of carbonates, since the parameters of  $\text{CO}_2$  desorption profiles ( $T_{\text{max}}$ , desorption range  $\Delta T$ , and the amount of desorbed molecules) for these samples differ when the content in zirconium supports changes, which affects the properties of surface oxygen involved in the formation of carbonate structures.

The effect of oxygen adsorption on the properties of carbonyl and carbonate complexes was studied. Figure 8 shows the TPD CO +  $\text{O}_2$  profiles. They were obtained after the adsorption of oxygen ( $P = 3 \times 10^2$  Pa,  $T = 20^\circ\text{C}$ ,  $\tau_{\text{ads}} = 10$  min) on samples with CO previously adsorbed on them under the conditions described above. The comparison of profiles in Figs. 7 and 8 and data in Tables 2 and 3 shows that, after  $\text{O}_2$  adsorption, the amount of desorbed CO decreases,

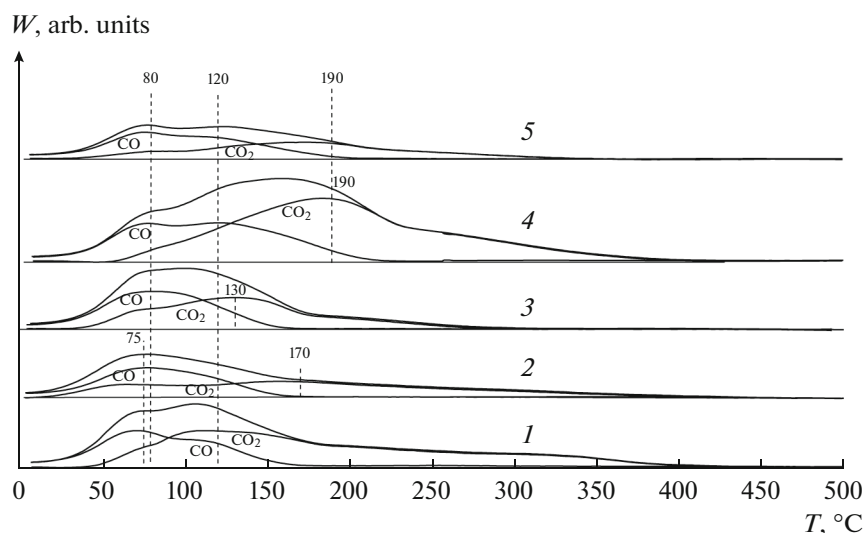


Fig. 7. TPD CO profiles for 5%CuO/CeO<sub>2</sub> (1), 5%CuO/Ce<sub>0.8</sub>Zr<sub>0.2</sub>O<sub>2</sub> (2), 5%CuO/Ce<sub>0.5</sub>Zr<sub>0.5</sub>O<sub>2</sub> (3), 5%CuO/Ce<sub>0.2</sub>Zr<sub>0.8</sub>O<sub>2</sub> (4), 5%CuO/ZrO<sub>2</sub> (5) samples.

and the desorbed CO<sub>2</sub> increases in the respective temperature ranges. That is, CO of carbonyl complexes is oxidized by adsorbed oxygen to form carbonates, the decomposition temperature of which is lower than the decomposition temperature of carbonates at the oxidation sites. The highest efficiency of the oxidation of CO in carbonyl complexes during oxygen adsorption is observed on the 5%CuO/CeO<sub>2</sub> sample. For it, as can be seen from Table 3, the ratio  $n$  of the amounts of desorbed CO in TPD CO and TPD CO + O<sub>2</sub> experiments is 4.5. For samples with  $x = 0.2-1$ , it ranges from 1.75 to 2.4.

On the 5%CuO/CeO<sub>2</sub> and 5%CuO/Ce<sub>0.8</sub>Zr<sub>0.2</sub>O<sub>2</sub> catalysts, part of the CO molecules in carbonyl complexes is oxidized by oxygen to CO<sub>2</sub> ( $2.7 \times 10^{19} \text{ g}^{-1}$ ) followed by its desorption at room temperature. The desorption of CO<sub>2</sub> is negligible in the case of samples with  $x \geq 0.5$  ( $0.47 \times 10^{19} \text{ g}^{-1}$ ). Treatment of samples with 5%CuO/Ce<sub>1-x</sub>Zr<sub>x</sub>O<sub>2</sub> with adsorbed CO with oxygen also lowers the decomposition temperature of surface carbonates at the oxidation sites by  $\sim 50^\circ\text{C}$ . This agrees with the data of [26], where it was shown

that, on the oxidized surface of 5%CuO/CeO<sub>2</sub>, the decomposition temperature of carbonates in CO<sub>2</sub> is lower than on the reduced one. Therefore, the combined oxidation of carbonyls and the catalyst occurs during oxygen adsorption.

Thus, carbonyl and carbonate complexes are formed at room temperature on the 5%CuO/Ce<sub>1-x</sub>Zr<sub>x</sub>O<sub>2</sub> samples during CO adsorption at the sites of adsorption and oxidation. Their thermal stability and amount depend on the zirconium content of CeO<sub>2</sub>. Carbonyls are oxidized to carbonates in the course of oxygen adsorption at 20°C. The decomposition temperature of these carbonates is lower than that of carbonates at the oxidation sites. In the 5%CuO/CeO<sub>2</sub> and 5%CuO/Ce<sub>0.8</sub>Zr<sub>0.2</sub>O<sub>2</sub> samples, oxygen oxidizes CO of carbonyl complexes to CO<sub>2</sub> even at room temperature. In parallel with the oxidation reaction of carbonyls to carbonates, the oxidation of catalysts takes place, which leads to a decrease in the temperature of decomposition of carbonates on them into CO<sub>2</sub> at the oxidation sites.

Table 2. TPD CO characteristics

Sample	CO		CO <sub>2</sub>		$N_{\text{des.CO+CO}_2} \times 10^{-18}, \text{ m}^{-2}$	$N_{\text{Cu+Zr}} / N_{\text{des.CO+CO}_2}$
	$T_{\text{max}}, ^\circ\text{C}$	$N_{\text{des.CO}} \times 10^{-18}, \text{ m}^{-2}$	$T_{\text{max}}, ^\circ\text{C}$	$N_{\text{des.CO}_2} \times 10^{-18}, \text{ m}^{-2}$		
5%CuOCeO <sub>2</sub>	75; 114	0.9	80; 110	1.8	2.7	3.7
5%CuO/Ce <sub>0.8</sub> Zr <sub>0.2</sub> O <sub>2</sub>	80	1.1	70; 168	1.3	2.4	5.4
5%CuO/Ce <sub>0.5</sub> Zr <sub>0.5</sub> O <sub>2</sub>	80	1.4	75; 130	1.5	2.8	5
5%CuO/Ce <sub>0.2</sub> Zr <sub>0.8</sub> O <sub>2</sub>	75; 120	1.2	190	2.3	3.5	2.6
5%CuO/ZrO <sub>2</sub>	80; 120	1.4	96; 180	1.5	2.9	6.6

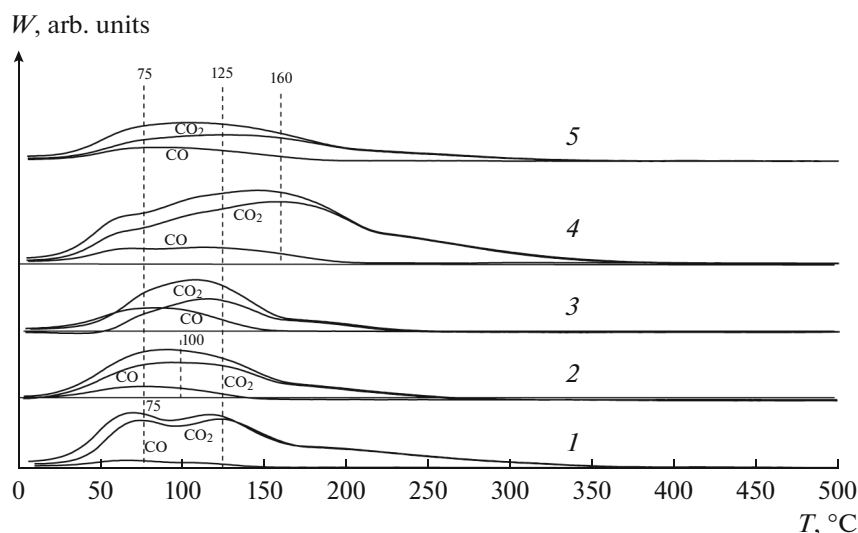


**Fig. 8.** TPD CO + O<sub>2</sub> profiles for 5%CuO/CeO<sub>2</sub> (1), 5%CuO/Ce<sub>0.8</sub>Zr<sub>0.2</sub>O<sub>2</sub> (2), 5%CuO/Ce<sub>0.5</sub>Zr<sub>0.5</sub>O<sub>2</sub> (3), 5%CuO/Ce<sub>0.2</sub>Zr<sub>0.8</sub>O<sub>2</sub> (4), 5%CuO/ZrO<sub>2</sub> (5) samples.

## DISCUSSION

### *CO Adsorption and Oxidation Sites on the 5%CuO/Ce<sub>1-x</sub>Zr<sub>x</sub>O<sub>2</sub> Samples*

We found earlier [12, 13] that with a copper oxide content of 0.5–15% for CuO/CeO<sub>2</sub> and CuO/ZrO<sub>2</sub> samples, the maximum number of CO chemisorption sites and active sites in selective CO oxidation is achieved at a CuO concentration of ~5%. The particles of the CuO phase and the CuO<sub>m</sub> oxo complexes in the above processes are inactive. Therefore, the participation of these particles in reactions with 5%CuO/Ce<sub>1-x</sub>Zr<sub>x</sub>O<sub>2</sub> is also unlikely. Highly dispersed copper oxide is present in all samples. Depending on the properties of the support, its temperature of reduction by hydrogen varies in the range of 145–194°C (Fig. 4). In this temperature region, various forms of CuO can be reduced: copper oxide, which strongly interacts with the support; small two- and three-dimensional copper oxide clusters, which weakly interact with the support; solid solutions; interstitial or substitution defects in the support lattice [28, 31].

We believe that, in the 5%CuO/CeO<sub>2</sub>, 5%CuO/Ce<sub>0.8</sub>Zr<sub>0.2</sub>O<sub>2</sub>, and 5%CuO/Ce<sub>0.5</sub>Zr<sub>0.5</sub>O<sub>2</sub> samples, the low-temperature peaks at 145, 163, and 194°C refer to the reduction of high-dispersity copper oxide, which strongly interacts with the supports [33, 35]. The reduction temperature of this form of CuO depends on the content of zirconium cations in the support and is not associated with changes in the specific surface areas of the samples. An increase in the temperature can be explained by an increase in the strength of oxygen binding in CuO upon its interaction with zirconium cations. This is supported by the fact that, on the surface of CeO<sub>2</sub> and ZrO<sub>2</sub>, the binding strength of charged oxygen forms and with Zr<sup>4+</sup> cations is higher than with Ce<sup>4+</sup> [36]. The above form of copper contains active oxygen on the interface between dimers or small CuO clusters with a support in –Cu–O–Ce– structures [11, 35]. This type of oxygen is associated with the low-temperature oxidation of CO on 5%CuO/CeO<sub>2</sub> and 5%CuO/Ce<sub>0.8</sub>Zr<sub>0.2</sub>O<sub>2</sub> [28].

The activity of the 5%CuO/ZrO<sub>2</sub>(m + t) sample in CO chemisorption at 20°C and in low-temperature

**Table 3.** TPD CO + O<sub>2</sub> characteristics

Sample	CO		CO <sub>2</sub>		$N_{\text{des.CO+CO}_2} \times 10^{-18}, \text{m}^{-2}$	$n$
	$T_{\text{max}}, ^\circ\text{C}$	$N_{\text{des.CO}} \times 10^{-18}, \text{m}^{-2}$	$T_{\text{max}}, ^\circ\text{C}$	$N_{\text{des.CO}_2} \times 10^{-18}, \text{m}^{-2}$		
5%CuOCeO <sub>2</sub>	71; 110	0.2	75; 123	2.1	2.3	4.5
5%CuO/Ce <sub>0.8</sub> Zr <sub>0.2</sub> O <sub>2</sub>	85	0.5	110	1.7	2.2	2.2
5%CuO/Ce <sub>0.5</sub> Zr <sub>0.5</sub> O <sub>2</sub>	90	0.8	120	1.0	1.8	1.75
5%CuO/Ce <sub>0.2</sub> Zr <sub>0.8</sub> O <sub>2</sub>	70; 120	0.5	164	2.6	3.1	2.4
5%CuO/ZrO <sub>2</sub>	93	0.8	130	2.3	3.1	1.75



oxidation of CO is associated with CuO oxide on  $ZrO_2(t)$  crystallites, since CuO on  $ZrO_2(m)$  is inactive in these reactions [13]. The authors of [37] believe that on the surface of the oxide  $ZrO_2(t)$  (the tetragonal phase in the sample was stabilized by the introduction of Y ions), oxygen vacancies (V) are present. Their interaction with oxygen of CuO clusters ( $-V-O^{2-}-Cu^{2+}-$ ) lowers the binding energy of oxygen with the copper cation and thus increases the reactivity of oxygen in the oxidation of CO compared with oxygen of the CuO phase. Apparently, the active oxygen of the above-mentioned copper-containing sites on the crystallites of the tetragonal  $ZrO_2$  phase of is responsible for the adsorption and oxidation of CO on 5%CuO/ $ZrO_2(m+t)$ . Active oxygen is involved in the reduction of CuO clusters with hydrogen at 170°C (Fig. 4).

In the 5%CuO/ $Ce_{0.2}Zr_{0.8}O_2(c)$  profile, three forms of CuO are reduced by  $H_2$  at 140, 175, and 240°C. The main peaks at 175 and 240°C are close to those on the profile for 5% CuO/ $ZrO_2(t)$  and correspond to the recovery of clusters and particles of the CuO phase. The peak at 140°C is probably associated with the  $-Cu-O-Ce-$  structure, since the peak at this temperature is on the TPR- $H_2$  curve of the 5%CuO/ $CeO_2$ . Therefore, in the 5%CuO/ $Ce_{0.2}Zr_{0.8}O_2(c)$  catalyst, active adsorption and CO oxidation sites are formed during the interaction of CuO clusters and vacancies on the surface of  $ZrO_2$  crystallites. The introduction of Ce cations in a low concentration into the support structure (when their amount is for times smaller than the number of Zr cations) stabilizes the cubic structure of zirconium oxide, which corresponds to that for nonstoichiometric  $ZrO_{1.87}(c)$  with a lattice parameter of 5.15 Å and a high content of oxygen vacancies [16]. This may contribute to an increase in the number of  $-V-O^{2-}-Cu^{2+}-$  sites in the catalyst 5%CuO/ $Ce_{0.2}Zr_{0.8}O_2(c)$ , and, consequently, its activity in adsorption and CO oxidation as compared with 5%CuO/ $ZrO_2(m+t)$ . The stabilization of zirconium oxide structure by Ce cations was reported in [7].

In oxidized 5%CuO/ $Ce_{1-x}Zr_xO_2$  samples, the oxidation sites  $Cu^{2+}O^{2-}$  contain the structures with active oxygen discussed above. During the adsorption of CO on them, complexes are formed during the transfer of oxygen atoms from  $Cu^{2+}O^{2-}$  to the created carbonate structures. In this reaction, part of the  $Cu^{2+}$  copper cations is reduced to  $Cu^+$  adsorption sites located near oxygen vacancies formed. Such a mechanism for the formation of CO adsorption sites was studied on the 5%CuO/ $CeO_2$  and 5%CuO/ $ZrO_2$  samples in [26, 27] and is valid for copper-containing catalysts prepared on the basis of solid solutions, since the observed patterns of CO and  $CO_2$  desorption for the 5%CuO/ $Ce_{1-x}Zr_xO_2$  samples with  $x = 0.2$  and 0.8 coincide with those for 5%CuO/ $CeO_2$  and 5%CuO/ $ZrO_2$ .

The efficiency of the formation of adsorption complexes at 20°C in catalysts can be judged by the ratio of the number of deposited copper cations  $N_{Cu^{2+}}$  to the value  $N_{des.CO+CO_2}$ , of the total number of desorbed CO +  $CO_2$  molecules for the samples. Table 2 shows that this ratio varies from 3 to 7 depending on the catalyst. For 5%CuO/ $Ce_{0.8}Zr_{0.2}O_2$ , 5%CuO/ $Ce_{0.5}Zr_{0.5}O_2$ , and 5%CuO/ $ZrO_2(m+t)$  samples, there are on average five to seven  $Cu^{2+}$  cations per adsorbed CO molecule. For 5%CuO/ $CeO_2$  and 5%CuO/ $Ce_{0.2}Zr_{0.8}O_2$  samples, the efficiency is higher, since the ratio is 3–4. The low efficiency of copper oxide in the formation of CO complexes may be due to the high oxygen binding strength in the CuO-phase particles and the lack of the access of CO molecules to copper oxide located inside the three-dimensional CuO structures or solid solution formed by copper oxide with a support.

Carbon monoxide in  $Cu^+-CO$  complexes is oxidized when oxygen is adsorbed to carbonates (Fig. 8). They decompose with  $CO_2$  desorption at a lower temperature than carbonates at the oxidation sites, which allows us to consider them as intermediates in the reaction of selective oxidation of CO with oxygen in a hydrogen-containing medium. The participation of strongly bound carbonates on the oxidation sites that decompose at  $T > 200^\circ C$  in the reaction of low-temperature CO oxidation is unlikely.

#### *On the Mechanism of CO Oxidation by Oxygen in the Presence of Hydrogen on 5%CuO/ $Ce_{1-x}Zr_xO_2$ Samples at Low Temperatures*

In the series of studied 5%CuO/ $Ce_{1-x}Zr_xO_2$  catalysts, the 5%CuO/ $CeO_2$  sample has the highest activity in the reaction of the selective oxidation of CO with oxygen in the excess of hydrogen. With an increase in the zirconium ion content of catalysts, the temperature of the onset of the reaction increases due to an increase in the strength of the oxygen bond in CuO [38]. A decrease in  $\gamma_{max}$  with increasing temperature corresponding to the maximum conversion can be explained by the competition for oxygen of the oxidation reactions of CO and  $H_2$  (Fig. 6). Copper oxide is reduced by hydrogen. It reduces the number of CO chemisorption sites, which, according to [12], leads to a decrease in the CO conversion.

The route of  $CO-Cu^+$  oxidation during oxygen adsorption plays a key role in the reaction of low-temperature oxidation of CO with oxygen in the presence of hydrogen on CuO/ $CeO_2$  catalysts. This is indicated by the correlation between the catalyst activity in the oxidation of CO and the concentration of  $Cu^+$  cations in it [4] and the overlap of the temperature ranges of CO conversion (40–160°C) and the decomposition of carbonates at the  $Cu^+$  adsorption sites (30–150°C) (Figs. 6 and 8). In the range from 100 to 220°C, the oxidation of CO with oxygen from oxidation sites also

contributes to the conversion due to a decrease in the decomposition temperature of carbonates at these sites by 50°C during oxygen adsorption.

The activated nature of the reaction is due to the conversion of carbonates to CO<sub>2</sub>, because the chemisorption of CO with the formation of carbonate and carbonyl complexes, the oxidation of carbonyl complexes and catalyst by oxygen occur at 20°C.

A similar mechanism for the oxidation of CO to CO<sub>2</sub> on 5%CuO/ZrO<sub>2</sub> was considered in [13]. In contrast to 5%CuO/CeO<sub>2</sub>, due to the higher strength of oxygen binding in carbonate complexes on the 5%CuO/ZrO<sub>2</sub>(t) sample, the oxidation of CO by the catalyst oxygen and gas phase oxygen under isothermal conditions takes place at a higher temperature: 100–220°C. The activity of the 5%CuO/Ce<sub>0.2</sub>Zr<sub>0.8</sub>O<sub>2</sub>(c) sample ( $\gamma_{\max} = 87\%$  at 160°C) is higher than that of 5%CuO/ZrO<sub>2</sub>(m + t) ( $\gamma_{\max} = 67\%$  at 180°C). This is probably due to the increase in the number of oxygen vacancies on the surface of the ZrO<sub>2</sub>(c) oxide involved in the formation of active oxygen in CuO. Excess vacancies are formed when the cerium cations stabilize the nonstoichiometric cubic structure of zirconium oxide.

## CONCLUSIONS

The 5%CuO/Ce<sub>1-x</sub>Zr<sub>x</sub>O<sub>2</sub> catalysts were synthesized on the basis of CeO<sub>2</sub>, ZrO<sub>2</sub>, and solid solutions Ce<sub>1-x</sub>Zr<sub>x</sub>O<sub>2</sub> with  $x = 0.2-0.8$  using the Pechini method.

A synergistic effect is observed in the 5%CuO/Ce<sub>1-x</sub>Zr<sub>x</sub>O<sub>2</sub> samples with  $x = 0, 0.2, \text{ and } 0.5$ : with an increase in the concentration of zirconium cations in them, the temperature of copper oxide and support reduction by hydrogen increases. The synergistic effect is small in the case of 5%CuO/Ce<sub>0.2</sub>Zr<sub>0.8</sub>O<sub>2</sub> and 5%CuO/ZrO<sub>2</sub>: the reduction temperature of copper oxide in them depends on the specific features of its interaction with the surface of crystallites of different phase composition.

Highly dispersed copper oxide is present in 5%CuO/Ce<sub>1-x</sub>Zr<sub>x</sub>O<sub>2</sub> catalysts. In strong interactions with supports, it forms active oxygen, which is involved in the chemisorption of CO and the low-temperature oxidation of CO in the presence of hydrogen.

The activity of 5%CuO/Ce<sub>1-x</sub>Zr<sub>x</sub>O<sub>2</sub> catalysts in the reaction of CO oxidation decreases with increasing zirconium content: the temperature of the onset of the reaction increases,  $\gamma_{\max}$  decreases with a shift in temperature corresponding to the maximum conversion to the high temperature region. The decrease in the activity of 5%CuO/CeO<sub>2</sub> during the modification of CeO<sub>2</sub> with Zr cations is due to the increase in the strength of oxygen binding in the copper-containing sites. The modification of ZrO<sub>2</sub> with cerium cations increases with the maximum conversion from 67% at

180°C to 87% at 160°C on the 5%CuO/Ce<sub>0.2</sub>Zr<sub>0.8</sub>O<sub>2</sub> sample as a result of an increase in the amount of oxygen vacancies involved in the formation of active oxygen in CuO.

Taking into account the properties of CO complexes formed on copper-containing oxidation and adsorption sites and interactions of complexes with adsorbed oxygen, their participation in the low-temperature oxidation reaction in hydrogen on 5%CuO/CeO<sub>2</sub> and 5%CuO/ZrO<sub>2</sub> catalysts was considered.

## ABBREVIATIONS AND NOTATION

$d$	size of particles
$c$	cubic modification of samples
$n$	amount of CO desorbed in TPD CO and TPD CO + O <sub>2</sub> experiments
$N_{\text{ads. CO}}$	amount of adsorbed CO
$N_{\text{des. CO}}$	amount of desorbed CO
$N_{\text{des. CO}_2}$	amount of desorbed CO <sub>2</sub>
$N_{\text{des. CO+CO}_2}$	overall amount of desorbed gas
$N_{\text{H}_2}$	overall amount of adsorbed hydrogen per square meter of the oxide
$N_r$	amount of hydrogen calculated by the reaction $\text{CuO} + \text{H}_2 = \text{Cu}^0 + \text{H}_2\text{O}$
$S_{\text{sp}}$	specific surface area
TPD	temperature-programmed desorption
TPR-H <sub>2</sub>	temperature-programmed reduction
$T_{\max}$	temperature corresponding to the maximal rate of desorption
$V$	oxygen vacancies
$w$	desorption rate
ZrO <sub>2</sub> (m)	monoclinic phases of ZrO <sub>2</sub>
ZrO <sub>2</sub> (t)	tetragonal phase of ZrO <sub>2</sub>
$\gamma_{\max}$	maximal conversion of CO

## FUNDING

This work was supported by grant no. 18-03-00627 A from the Russian Foundation for Basic Research and was carried out as part of the state assignment of the FASO Russia (theme V.46. 13, 0082-2014-0007, registration no. AAAA-A18-118020890105-3).

## REFERENCES

- Mishra, A. and Prasad, R., *Bull. Chem. React. Eng. Catal.*, 2011, vol. 6, no. 1, p. 1.
- Olah, D., Goepfert, A., and Surya Prokash, G.K., *Beyond Oil and Gas: The Methanol Economy*, Weinheim: Wiley, 2009.
- Avgouropoulos, G. and Ioannides, T., *Appl. Catal., A*, 2003, vol. 244, p. 155.
- Martinez-Arias, A., Gamarra, D., Hungria, A.B., Fernandez-Garcia, M., Munuera, G., Hornes, A., Bera, P.,

- Conesa, J.C., and Camara, A.L., *Catalysts*, 2013, vol. 3, p. 378.
5. Firsova, A.A., Il'ichev, A.N., Khomenko, T.I., Gorobinskii, L.V., Maksimov, Yu.V., Suzdalev, I.P., and Korchak, V.N., *Kinet. Catal.*, 2007, vol. 48, no. 2, p. 282.
  6. Balducci, G., Islam, M.S., Kaspar, J., Fornasiero, P., and Graziani, M., *Chem. Mater.*, 2003, vol. 15, p. 3781.
  7. Kaspar, J., Fornasiero, P., and Hickey, N., *Catal. Today*, 2003, vol. 77, p. 419.
  8. Cao, J.-L., Wang, Y., Zhang, T.-Y., Wu, S.-H., and Yuan, Z.-Y., *Appl. Catal., B*, 2008, vol. 78, p. 120.
  9. Manzoli, M., Monte, R.D., Boccuzzi, F., Coluccia, S., and Kaspar, J., *Appl. Catal., B*, 2005, vol. 61, p. 192.
  10. Ratnasamy, P., Strinivas, D., Satyanarayana, C.V.V., Manikandan, P., Kumaran, R.S.S., Sachin, M., and Shetti, V.N., *J. Catal.*, 2004, vol. 221, p. 455.
  11. Martinez-Arias, A., Fernandez-Garcia, M. Galvez, O., Coronado, J.M., Anderson, J.A., Conesa, J.C., Soria, J., and Munuera, G., *J. Catal.*, 2000, vol. 195, p. 207.
  12. Il'ichev, A.N., Firsova, A.A., and Korchak, V.N., *Kinet. Catal.*, 2006, vol. 47, no. 4, p. 585.
  13. Il'ichev, A.N., Bykhovskii, M.Ya., Fattakhova, Z.T., Shashkin, D.P., Matyshak, V.A., and Korchak, V.N., *Kinet. Catal.*, 2018, vol. 59, no. 2, p. 179.
  14. Firsova, A.A., Khomenko, T.I., Il'ichev, A.N., and Korchak, V.N., *Kinet. Catal.*, 2011, vol. 52, no. 3, p. 434.
  15. Sadykov, V.A., Simonov, M.N., Mezentseva, N.V., Pavlova, S.N., Fedorova, Y.E., Bobin, A.S., Bessalko, Y.N., Ishchenko, A.V., Krieger, T.A., Glazneva, T.S., Larina, T.V., Cherepanova, S.V., Kaichev, V.V., Saraev, A.A., Chesalov, Y., Shmakov, A.N., Roger, A.-C., and Adamski, A., *Open Chem.*, 2016, vol. 14, p. 363.
  16. *Powder Diffraction File. Alphabetical Indexes. Inorganic phases*, JCPDS, Pennsylvania: International Center for Diffraction Data, 1983.
  17. Mirkin, L.I., *Spravochnik po rentgenostruktturnomu analizu polikristallov* (Polycrystals X-ray Diffraction Handbook), Moscow: Gos. Izd. Fiz.-Mat. Lit., 1961.
  18. Tret'yakov, I.I., Shub, B.R., and Sklyarov, A.V., *Zh. Fiz. Khim.*, 1970, vol. 44, p. 2112.
  19. *Handbuch der Präparativen Anorganischen Chemie*. Brauer, G., 1962, Stuttgart: Ferdinand Enke-Verlag.
  20. Rodriguez, J.A. Hanson, J.C. Kim, J.-Y. Liu, G., Iglesias-Juez, A., and Fernandez-Garcia, M., *J. Phys. Chem. B*, 2003, vol. 107, p. 3535.
  21. Narula, C.K., Haack, L.P., Chun, W., Jen, H.-W., and Graham, G.W., *J. Phys. Chem. B*, 1999, vol. 103, p. 3634.
  22. Trovarelli, A., Zamar, F., Llorca, J., Leitenburg, C., Dolcetti, G., and Kiss, J.T., *J. Catal.*, 1997, vol. 169, p. 490.
  23. Fornasiero, P., Balducci, G., Monte, R.D., Kaspar, J., Sergo, V., Gubitosa, G., Ferrero, A., and Graziani, M., *J. Catal.*, 1996, vol. 164, p. 173.
  24. Fully, F., Perrichon, V., Vidal, H., Kaspar, J., Blanco, G., Pintado, J.M., Bernal, S., Golon, G., Daturi, M., and Lavalley, J.C., *Catal. Today*, 2000, vol. 59, p. 373.
  25. Maity, S.K., Rana, M.S., Srinavas, B.N., Bej, S.K., Dhar, G.M., and Prasada Rao, T.S.R., *J. Mol. Catal. A: Chem.*, 2000, vol. 153, p. 121.
  26. Il'ichev, A.N., Matyshak, V.A., and Korchak, V.N., *Kinet. Catal.*, 2015, vol. 56, no. 1, p. 115.
  27. Il'ichev, A.N., Shashkin, D.P., Matyshak, V.A., and Korchak, V.N., *Kinet. Catal.*, 2015, vol. 56, no. 2, p. 197.
  28. Luo, M.F., Ma, J.-M., Lu, J.-Q., Song, Y.-P., and Wang, Y.-J., *J. Catal.*, 2007, vol. 246, p. 52.
  29. Gomez-Cortes, A., Marquez, Y., Arenas-Alatorre, J., and Diaz, G., *Catal. Today*, 2008, vols. 133–135, p. 743.
  30. Polster, C.S., Naier, H., and Baertsch, C.D., *J. Catal.*, 2009, vol. 266, p. 308.
  31. Moretti, E., Storaro, L., Talon, A., Lenarda, M., Riello, P., Frattini, R., Yuso, M.V.M., Jimenez-Lopez, A., Rodriguez-Gastellon, E., Ternero, F., Caballero, A., and Holgado, J.P., *Appl. Catal., B*, 2011, vol. 102, p. 627.
  32. Arango-Diaz, A., Cecilia, J.A., Moretti, E., Talon, A., Nunez, P., Morrero-Jerez, J., Jimenez-Jimenez, J., Jimenez-Lopez, A., and Rodriguez-Gastellon, E., *Int. J. Hydrogen Energy*, 2014, vol. 39, p. 4102.
  33. Wang, S.-P., Zheng, X.-C., Wang, X.-Y., Wang, S.-R., Zhang, S.-M., Yu, L.-H., Huang, W.-P., and Wu, S.-H., *Catal. Lett.*, 2005, vol. 105, nos. 3–4, p. 163.
  34. Dow, W.-P. and Huang, T.-J., *J. Catal.*, 1996, vol. 160, p. 171.
  35. Dow, W.-P., Wang, Y.P., and Huang, T.-J., *Appl. Catal., A*, 2000, vol. 190, p. 25.
  36. Il'ichev, A.N., Shashkin, D.P., Khomenko, T.I., Fattakhova, Z.T., and Korchak, V.N., *Kinet. Catal.*, 2010, vol. 51, no. 5, p. 743.
  37. Dow, W.-P., Wang, Y.P., and Huang, T.-J., *J. Catal.*, 1996, vol. 160, p. 155.
  38. Krylov, O.V., *Geterogennyi kataliz* (Heterogeneous Catalysis), Moscow: Akademkniga, 2004.